BRAIN
ORIGINAL ARTICLE

Cerebrospinal fluid immunoglobulins in primary progressive multiple sclerosis are pathogenic

Jamie K. Wong, Jerry Lin, Nathan J. Kung, Alexandra L. Tse, Serena J. E. Shimshak, Anna K. Roselle, Francesca M. Cali, Jessie Huang, Joseph M. Beaty, Taylor M. Shue and Saud A. Sadiq

See Guo and Lennon (https://doi.org/10.1093/brain/awad107) for a scientific commentary on this article.

Multiple sclerosis is clinically characterized by relapses and remissions (relapsing-remitting multiple sclerosis) that over time may evolve to a progressive course (secondary progressive multiple sclerosis) or as having a progressive course from disease onset (primary progressive multiple sclerosis). At present, it is not definitively known whether these clinical entities constitute a single pathological disease or whether these manifestations represent two distinct disease entities sharing inflammatory demyelination as a pathological feature. Here we show using a novel mouse model that CSF of primary progressive multiple sclerosis patients is unique in its capacity to induce motor disability and spinal cord pathology including demyelination, impaired remyelination, reactive astrogliosis and axonal damage. Notably, removal of immunoglobulin G from primary progressive multiple sclerosis CSF via filtration or immunodepletion attenuates its pathogenic capacity. Furthermore, injection of recombinant antibodies derived from primary progressive multiple sclerosis CSF recapitulates the pathology. Our findings suggest that the clinical and pathological features of primary progressive multiple sclerosis are antibody-mediated and pathogenically distinct from relapsing-remitting and secondary progressive multiple sclerosis. Our study has potentially important implications for the development of specific therapies for patients with primary progressive multiple sclerosis.

Tisch Multiple Sclerosis Research Center of New York, New York, NY 10019, USA

Correspondence to: Dr Saud A. Sadiq
Tisch Multiple Sclerosis Research Center of New York
521 West 57th Street, 4th floor, New York, NY 10019, USA
E-mail: ssadiq@tischms.org

Keywords: primary progressive multiple sclerosis; CSF; antibodies

Introduction

Multiple sclerosis is characterized by inflammatory demyelination, astrogliosis, microglial activation and axonal loss in the CNS, which ultimately leads to progressive clinical disability. The majority of patients initially present with relapsing-remitting multiple sclerosis (RRMS), where periods of neurological decline are interspersed with periods of clinical stability. Over time, many patients evolve to a phase of disease progression and clinical disability and are classified as having secondary progressive multiple sclerosis (SPMS). However, approximately 10–15% of patients have clinical disease progression and accumulating disability from disease onset and are diagnosed with primary progressive multiple sclerosis (PPMS).[1]

Although disease-modifying therapies that target the immune system have been effective in reducing relapses for the majority of RRMS patients, they do not halt disease progression in PPMS

Received August 10, 2022. Revised January 11, 2023. Accepted January 21, 2023. Advance access publication February 3, 2023

Table 1 Patient demographics for CSF samples used for intrathecal injections

Diagnosis	PPMS	RRMS	SPMS	HC
Number of patients (CSF samples)	10	8	8	3
Age at sample collection, mean (SD), years	55.4 (9.2)	39.9 (15.2)	61.9 (10.8)	54.7 (19.7)
Gender distribution	4 F; 6 M	8 F; 0 M	6 F; 2 M	2 F; 1 M
EDSS at sample collection, mean (SD)	5.7 (2.3)	1.6 (2.3)	5.7 (0.9)	N/A
Disease duration at sample collection, mean (SD), years	9.5 (6.7)	6.4 (10.6)	11.6 (12.0)	N/A
CSF cell count per ml, mean (SD)	1486 (1107)	4576 (3847)	3569 (5335)	4078
CSF protein concentration, mean (SD), µg/ml	945.9 (248.1)	792.1 (176.1)	872.32 (255.5)	850.8 (250.2)

EDSS = Expanded Disability Status Scale; SD = standard deviation.

Table 2 Patient demographics for rAbs used for intrathecal injections

Diagnosis	PPMS	RRMS	SPMS	DC (HTLV-1 and ALS)
Number of patients	7	4	4	3
Number of rAbs	13	4	4	3
Age at sample collection, mean (SD), years	42.8 (11.7)	37.8 (15.3)	51.0 (11.2)	56.7 (8.4)
Gender distribution	3 F; 4 M	3 F; 1M	1 F; 3 M	2 F; 1 M
EDSS at sample collection, mean (SD)	2.4 (2.0)	0.3 (0.6)	6.6 (0.6)	N/A
Disease duration at sample collection, mean (SD), years	2.8 (3.2)	0.3 (0.6)	23.7 (6.7)	N/A
CSF cell count per ml, mean (SD)	12 977 (17 861)	13 238 (21 848)	2966 (2518)	1109 (131)
rAb concentration, mean (SD), µg/ml	645.3 (290.6)	523.7 (191.1)	642.6 (213.8)	621.4 (109.3)

ALS = amyotrophic lateral sclerosis; DC = disease control; EDSS = Expanded Disability Status Scale; F = female; HTLV-1 = human T-lymphotropic virus type 1; M = male; rAb = recombinant antibody.

patients, suggesting that there are pathophysiological differences between RRMS and PPMS.[2,3] Indeed, lesions in PPMS patients tend to contain fewer inflammatory cells than in other multiple sclerosis subtypes.[4,5] Also, PPMS patients tend to have fewer and smaller brain lesions relative to RRMS/SPMS patients, with the brunt of the lesions and atrophy predominantly affecting the cervical spinal cord.[6-10] A better understanding of the pathological mechanisms underlying PPMS has been limited because the most commonly used experimental model of multiple sclerosis, experimental autoimmune encephalomyelitis (EAE), is more analogous to RRMS than PPMS. Thus, many of the therapies effective in treating EAE have proven efficacious in RRMS but not PPMS.[11,12]

Previous *in vitro* studies have reported that PPMS CSF can trigger apoptosis of neuronal cultures and branching of oligodendrocyte progenitor cells (OPCs); however, the identity of the PPMS CSF components mediating these effects remain unknown.[13,14] Ceramides in multiple sclerosis CSF have been reported to mediate mitochondrial dysfunction and axonal damage in rat hippocampal neuronal cultures.[15,16] We have previously shown the feasibility of using CSF obtained from multiple sclerosis patients as a vehicle to transmit pathology to mice. Injections of CSF derived from untreated PPMS patients into the third ventricle resulted in demyelinating lesions in the brain; however, only 12% of these mice developed lesions in the spinal cord and none exhibited any functional deficits.[17]

In this study, we administered CSF obtained from PPMS patients directly into the cervical subarachnoid space in mice. We found that a single intrathecal injection of PPMS CSF was able to induce forelimb motor deficits and characteristic cervical spinal cord pathology including: demyelination, reactive astrogliosis, microglial activation and axonal damage. Intriguingly, however, intrathecal delivery of CSF from RRMS and SPMS patients failed to induce these pathological effects, with the exception of mild microglial activation, which highlights fundamental differences between PPMS and RRMS/SPMS. Using our novel animal model of PPMS, we sought to identify the pathogenic component(s) in CSF contributing to disease pathology and assess the efficacy of using selective filtration as a therapeutic approach to eliminate putative pathogenic component(s) from PPMS CSF.

Materials and methods

Multiple sclerosis patient selection and CSF collection

CSF samples were collected from 42 patients with clinically definite multiple sclerosis,[18] two patients with amyotrophic lateral sclerosis (ALS) and one human T-lymphotropic virus type 1 (HTLV-1) patient as disease controls (DC), and four non-multiple sclerosis healthy controls (HC) at the International Multiple Sclerosis Management Practice following Institutional Review Board approval and informed consent according to the Declaration of Helsinki. The entire multiple sclerosis patient cohort included 17 PPMS, 13 RRMS and 12 SPMS patients (Tables 1 and 2 and Supplementary Tables 1–3). None of the multiple sclerosis patients received any kind of immunomodulatory treatment for at least 6 months prior to CSF collection. Samples were collected with sterile techniques either by lumbar puncture or by aspiration from access ports of previously implanted baclofen pumps. CSF samples were centrifuged at 200 *g* for 15 min to remove cells, then stored in aliquots at −80°C. All samples used in this study were free of red blood cell contamination.

Cervical subarachnoid space injections in mice

Adult female C57BL/6J mice (aged 8–10 weeks) purchased from The Jackson Laboratory (Bar Harbor, ME) were used in all *in vivo* experiments. All procedures were approved by the Institutional Animal Care and Use Committee at Mispro Biotech Services (New York). Mice were anaesthetized intraperitoneally with a ketamine (110 mg/kg) and xylazine (10 mg/kg) cocktail and given

subcutaneous injections of 0.1 mg/kg buprenorphine, 2.5 mg/kg baytril and 1 ml 0.9% saline pre-surgery. Laminectomies at cervical levels 4 (C4) and 5 (C5) were performed to expose the underlying dura mater and spinal cord. Using a 32-gauge Hamilton syringe, 3 µl of either CSF, filtered PPMS CSF, immunoglobulin G (IgG)-depleted PPMS CSF, recombinant antibodies (rAbs) or saline was injected into the subarachnoid space. Mice were assigned to different treatment groups in a randomized manner. A minimum of three mice were injected per each unpooled, individual CSF sample or rAb sample (except for four rAbs; Supplementary Table 4).

Lysolecithin injection

Mice were anaesthetized and given preoperative drugs, as described above. Mice underwent a C5 laminectomy and 1 µl of 1% lysolecithin (Sigma-Aldrich) dissolved in 0.9% saline was stereotaxically injected into the dorsal column at a depth of 0.5 mm using a 33-gauge Hamilton syringe. At 5 days post lysolecithin injection, mice underwent a second surgery for intrathecal delivery of CSF or saline at the site of focal demyelination. Following a C4 laminectomy, a 32-gauge Hamilton syringe was inserted underneath the dura mater and 3 µl CSF or saline was injected into the subarachnoid space. Mice were assigned to different treatment groups in a randomized manner. Mice were perfused for histological analyses at 1 week post CSF injection, as described below. A separate cohort of mice for a longer time-course study was perfused at 27 days post CSF injection.

Behavioural testing

Motor deficit score testing

All motor testing was performed blinded with respect to treatment groups. Following intrathecal delivery of CSF, mice underwent motor testing at 1 day post injection (DPI), 3 DPI and 7 DPI. Forelimb reaching, gripping and tail flaccidity were evaluated on a 3-point scale. Mice were held by their tails next to their cage bars and allowed to reach out and grip the bars for five trials. Mice exhibiting normal motor function were given a score of 0. Any deficits in either reaching or gripping were each given a score of 1. Specifically, an inaccurate reach was considered to be a reaching deficit, and weakness in grip strength or clenched forepaws were scored as gripping deficits. Tail flaccidity was also given a score of 1.

Grip strength testing

Mice were habituated to the grip strength meter (TSE systems) for 3 days prior to surgery. Each mouse was given 1 min to explore the grip strength meter, then held by their tails and allowed to grip the bar with both forelimbs for five consecutive trials. After a 30-s rest period, the mouse was given another five trials to grip, then returned to their home cage. Baseline grip strength force was measured at 1 day prior to surgery and grip strength was also measured at 1 DPI. The mean grip strength force was calculated from five trials and normalized grip strength values were calculated by dividing mean grip strength force measured at 1 DPI by mean grip strength force measured pre-surgery.

Tissue harvesting

Mice received an overdose of ketamine (300 mg/kg) and xylazine (30 mg/kg) and were perfused transcardially at 1 DPI, 3 DPI, 7 DPI or 27 DPI with PBS followed by 4% paraformaldehyde in 0.1 M PBS, pH 7.4. Brains and spinal cords were dissected out, postfixed in 4% paraformaldehyde overnight, then placed in 30% sucrose overnight for cryoprotection.

Histology

For mice that received a single intrathecal injection, spinal cords were cut 0.5 cm rostral and 0.5 cm caudal to the injection site. The 1 cm segments were then embedded and frozen in Tissue Tek® (VWR International). Spinal cords were sectioned sagittally at 20 µm thickness using a cryostat (Leica), then slide-mounted onto Histobond® slides (VWR International). Brains were sectioned in the coronal plane at 20 µm thickness and collected free-floating in 0.01% sodium azide in PBS.

For mice that received a lysolecithin injection followed by intrathecal delivery of CSF, an 8 mm segment of cervical spinal cord was embedded and frozen in Tissue Tek®. Spinal cords were sectioned coronally at 20 µm thickness using a cryostat, then slide-mounted onto Histobond® slides.

Immunofluorescence staining

Slides containing tissue sections or cells, or free-floating brain sections were washed three times in 0.1% Triton X-100 in PBS (PBS/T), then incubated in 10% normal goat serum (NGS) in PBS/T for 1 h at room temperature. Primary antibodies were diluted in 10% NGS in PBS/T and incubation occurred overnight at 4°C. The next day, sections were rinsed three times in PBS then incubated in a 1:750 dilution of the appropriate Alexa-Fluor secondary antibodies (Invitrogen) in 10% NGS in PBS/T for 1.5 h at room temperature. Sections were rinsed three times in PBS, then counterstained with DAPI in PBS (Invitrogen, 1:2500) for 5 min. After two final washes in PBS, slides were mounted using Fluoromount (Sigma-Aldrich).

Primary antibodies used include: mouse GFAP for astrocytes (Novus Biologicals, 1:500), rabbit Iba1 for microglia (Wako, 1:500), mouse SMI-32 for non-phosphorylated neurofilament-H (Covance, 1:1000), rabbit GLT-1 for glutamate transporter-1 (Abcam, 1:200), mouse APC for mature oligodendrocytes (Calbiochem, 1:100), rabbit Olig2 for oligodendrocyte lineage cells (Millipore, 1:500), rabbit NG2 for OPCs (Millipore, 1:200), rat Ki67 (ThermoFisher, 1:100) and rabbit Ki67 for cell proliferation (Abcam, 1:200).

To detect human IgG staining, the same procedure was followed, except overnight incubation occurred in 10% NGS in PBS/T without any primary antibody, and Alexa-Fluor goat anti-human IgG secondary antibody (Invitrogen, 1:750) was used.

Luxol fast blue staining

Slides were washed in PBS, then water before immersing in 70% ethanol, 80% ethanol, then 90% ethanol twice, for 5 min each. Slides were incubated in 0.1% Luxol fast blue (LFB; Electron Microscopy Sciences) in 95% ethyl alcohol with acetic acid at 60°C for 2.5 h. Excess staining was removed by rinsing slides in water. Staining was then differentiated by immersing slides in 0.05% lithium carbonate (ACROS H_2O Organics). Slides were then stained in 0.5% cresyl violet (Sigma). After rinsing in water, slides were dehydrated in three washes each of: 70%, 90% and 100% ethanol for 5 min. Slides were cleared in three washes of xylene for 5 min each, then mounted using cytoseal (Thermo Scientific).

Histological analyses

All imaging and quantification were performed by experimenters blinded for treatment groups. Images were captured using an Olympus microscope or a Zeiss Axio Imager. Acquisition parameters and exposure times were kept consistent for each immunostaining analysis. Images were taken at ×20 magnification and ImageJ software was used for all analyses. Immunostaining intensities were quantified in the dorsal white matter of the cervical spinal cord or in the corpus callosum. Total demyelination volume in lysolecithin-injected mice was quantified by measuring the area of demyelination determined by LFB staining at least every 480 µm throughout the entire lesion, then multiplying area by distance between sections. GFAP and Iba1 immunostaining intensities (mean grey values) in lysolecithin-injected mice were measured in the dorsal column at a maximum interval of 480 µm, throughout the entire lesion (estimated by referring to LFB staining). The number of proliferating OPCs or number of mature oligodendrocytes was determined by counting the number of cells in the dorsal column expressing both NG2 and Ki67 or APC and Olig2, respectively, at a maximum interval of 480 µm throughout the entire lesion.

RNA extraction

The cervical region of the spinal cord (C1 to C5) was dissected out at 1 day post intrathecal CSF delivery. Fresh spinal cords were placed on dry ice then processed for RNA extraction using the RNeasy Lipid Tissue Mini Kit (Qiagen), according to manufacturer instructions.

Quantitative real-time PCR

Quantitative real-time PCR (q-RT-PCR) was performed using the Applied Biosystems 7900 HT Fast Real-Time PCR system with individual TaqMan probes (Applied Biosystems). The ΔΔCt method was used to calculate fold changes in RNA expression, with the saline group as the calibrator and β-actin as the internal control.

CSF treatment on human astrocyte cultures

Human cortical astrocytes (Lonza) were plated at a density of 10 000 cells/cm^2 in either 6-well plates for RNA extraction or 8-well chamber slides for immunocytochemistry. Astrocytes were cultured in AGM^{TM} astrocyte growth medium (Lonza) containing 3% foetal bovine serum until they reached 80–90% confluence. CSF diluted at a ratio of 1:1 in DMEM was applied to astrocytes. After 24 h, astrocytes were either processed for RNA extraction using the RNeasy Plus Micro Kit (Qiagen) according to manufacturer instructions, or fixed with 4% paraformaldehyde for immunocytochemistry.

CSF filtration studies

CSF samples from PPMS patients underwent tangential flow filtration using either 5 kDa or 100 kDa MWCO hollow-fibre filters (Spectrum). Filters were primed with sterile-filtered distilled H_2O prior to sample filtration. CSF was passed through the filters at a flow rate of 0.7 ml/min using a peristaltic pump for 3 filtration cycles (Watson Marlow), then stored in aliquots at −80°C until use. CSF protein concentrations were measured using a Pierce BCA protein assay according to manufacturer instructions (Thermo Fisher Scientific). Unfiltered and filtered PPMS CSF samples were injected intrathecally into mice, or applied on human astrocyte cultures, as described above.

IgG depletion from CSF

PPMS CSF samples were incubated with Dynabeads^{TM} Protein A (Thermo Fisher Scientific) for 1 h at 4°C to remove IgGs. The IgG-depleted CSF was then centrifuged in an ultrafree-MC centrifugal filter tube at 12 000 *g* at 4°C for 6 min. Samples were stored at −80°C until use.

Coomassie staining

Unfiltered, filtered and IgG-depleted CSF samples were run on a NuPAGE^{TM} 4–12% bis-tris protein gel (Thermo Fisher Scientific) then placed in 25% isopropanol with 10% acetic acid for 30 min. The gel was stained in 0.006% Coomassie Brilliant Blue in 10% acetic acid overnight at room temperature. Following destaining with 10% acetic acid, the gel was rinsed in H_2O. Images of gels were captured using Carestream MI system and software.

Recombinant antibodies

Single cell analysis and sequencing of immunoglobulin genes of multiple sclerosis CSF B-cells yielded paired light chain and heavy chain variable regions. Sequences were then combined with published sequences of immunoglobulin heavy constant gamma 1 and the appropriate kappa or lambda light chain constant regions for full recombinant human IgG_1 antibody expression. Expression vectors with full heavy and light chains were transfected into Freestyle HEK 293-F cells (Thermo Fisher). Transfected cells were incubated at 37°C and 8% CO_2 with constant shaking for 5–7 days for antibody expression. Secreted antibodies were then purified via a protein G agarose column. Purified antibodies were then dialysed into PBS. Detailed methods are described in the Supplementary material.

Statistical analyses

GraphPad Prism 8 software was used to perform statistical analyses. Motor deficit scores, normalized grip strength, immunostaining intensities, cell counts and relative mRNA levels were analysed using a one-way ANOVA, with Bonferroni *post hoc* analyses. Protein concentrations were analysed using a paired, two-tailed Student's *t*-test. Statistical significance was determined by $P < 0.05$. Data are presented as mean ± SEM.

Data availability

Data reported in this manuscript are available from the corresponding author, upon reasonable request.

Results

Intrathecal injection of PPMS CSF induces motor disability and hallmark multiple sclerosis pathology

To determine whether intrathecal injection of PPMS CSF at C4-C5 would induce functional deficits in mice, we evaluated forelimb reaching, gripping and tail flaccidity at 1 DPI, 3 DPI and 7 DPI of CSF from patients of different multiple sclerosis subtypes and HCs (Table 1). We found inaccurate forelimb reaching, weaker grip strength, and increased tail flaccidity in PPMS CSF-injected mice by 1 DPI which persisted at 3 DPI and 7 DPI (one-way ANOVA; $P = < 0.0001$ for 1 and 3 DPI, $P = 0.0001$ for 7 DPI; Fig. 1A–C). However, motor deficit scores in mice injected with CSF from RRMS and SPMS patients were similar to mice injected with saline or

control CSF from healthy individuals. Deficits were not due to a quantitative effect, as no correlation was found between CSF IgG concentration and the development of these clinical effects. Indeed, RRMS or SPMS CSF with higher IgG concentrations (compared to PPMS CSF) did not induce pathological effects.

Histology was performed to assess whether PPMS CSF-induced motor impairments were associated with cervical cord changes at the site of CSF injection. LFB staining revealed distinct demyelinated lesions only in PPMS CSF-injected mice, while myelin remained intact in all other groups (Fig. 1D). Additionally, only spinal cords of PPMS CSF-injected mice exhibited reactive astrogliosis indicated by upregulated GFAP expression (one-way ANOVA; $P = 0.0001$; Fig. 1D and E). Time course analysis showed that by 1 DPI, GFAP expression was already significantly upregulated in PPMS CSF-injected mice as compared to all other groups (one-way ANOVA; $P = 0.0297$; Supplementary Fig. 1B). At 3 DPI, GFAP expression was higher in PPMS CSF-injected mice, but differences did not reach statistical significance (one-way ANOVA; $P = 0.3038$; Supplementary Fig. 1B). At 7 DPI, GFAP expression remained elevated in PPMS CSF-injected mice and immunostaining intensity was significantly higher than other groups (one-way ANOVA; $P = 0.0007$; Supplementary Fig. 1B). These findings were corroborated in a separate cohort of PPMS CSF-injected mice which also showed significantly upregulated *GFAP* mRNA expression in the cervical spinal cord at 1 DPI (one-way ANOVA; $P = 0.0147$; Supplementary Fig. 1A). Although Iba1$^+$ immunostaining intensity appeared similar in all groups, morphological changes indicative of microglial activation were observed in PPMS and SPMS CSF-injected mice, but to a lesser extent in RRMS CSF-injected mice (Fig. 1D and F and Supplementary Fig. 1E).

To verify whether the specific effects of PPMS CSF on astrocytes also occur on human cells, primary human astrocytes were incubated in 50% CSF from different multiple sclerosis subtypes for 1 day. PPMS CSF induced significantly higher numbers of GFAP$^+$Ki67$^+$ proliferating astrocytes and elevated Ki67 mRNA expression, while RRMS, SPMS and HC CSF had no effect on astrocyte proliferation, confirming that the induction of reactive astrogliosis is unique to PPMS CSF (Supplementary Fig. 2A–C). Levels of *STAT3* and *IL-6* mRNA expression were similar in all groups, suggesting that PPMS CSF-induced astrocyte proliferation occurs via STAT3-independent signalling pathways (Supplementary Fig. 2E and F).

In multiple sclerosis patients, motor disability typically correlates with spinal cord atrophy due to axonal loss.[19,20] To investigate whether the motor deficits induced by PPMS CSF were also associated with underlying axonal damage in the spinal cord, SMI-32 immunostaining was performed to assess levels of non-phosphorylated neurofilament heavy chain. The intensity of SMI-32 immunostaining in the dorsal white matter was significantly higher in PPMS CSF-injected mice, as compared to saline-injected mice (one-way ANOVA; $P = 0.0062$; Fig. 1D and G). Time course analysis revealed that SMI-32 expression was significantly upregulated compared to other treatment groups at 1 DPI (one-way ANOVA; $P = 0.0041$; Supplementary Fig. 1C). However, although SMI-32 expression remains elevated in PPMS CSF-injected mice at 3 DPI and 7 DPI, differences in SMI-32 expression between groups were not statistically significant (one-way ANOVA; $P = 0.1860$ and $P = 0.3926$, respectively; Supplementary Fig. 1C).

Additionally, excitotoxic cell death may be one of the mechanisms underlying multiple sclerosis pathology as glutamate transporter-1 (GLT-1) downregulation in multiple sclerosis lesions has been previously reported.[21] To determine whether axonal damage in PPMS CSF-injected mice was associated with excitotoxicity-induced changes, GLT-1 immunostaining was performed on cervical spinal cords. PPMS CSF may be inducing excitotoxic effects as GLT-1 expression was significantly upregulated in PPMS CSF-injected mice, perhaps as a compensatory response (one-way ANOVA; $P = 0.0336$; Fig. 1D and H and Supplementary Fig. 1D). However, the extent of GLT-1 upregulation was insufficient to protect against damage in PPMS CSF-injected mice, suggesting that other mechanisms are likely involved.

Pathological changes induced by a single 3 µl intrathecal injection of PPMS CSF into the cervical subarachnoid space appeared to be restricted to the spinal cord, as these changes were not detected in the brain (Supplementary Fig. 1F–I). The motor impairments and histopathological changes observed only in spinal cords of PPMS CSF-injected mice suggest that the pathogenic capacity of CSF is unique to PPMS and that pathogenic components circulating in PPMS CSF may be triggering and/or exacerbating neurological damage underlying the unrelenting disease progression in PPMS. However, this does not exclude the possibility that other shared non–CSF-mediated pathological mechanisms exist between PPMS, RRMS and SPMS.

PPMS CSF delays remyelination in a lysolecithin-induced focal lesion

Because remyelination failure is thought to underlie the non-relapse progression in PPMS, we investigated whether PPMS CSF negatively impacts the spontaneous remyelination that normally occurs following lysolecithin-induced demyelination. Mice received an intrathecal injection of PPMS CSF 5 days after an intraspinal injection of lysolecithin, near the stage of peak demyelination (Supplementary Table 1). Lysolecithin-injected mice that received intrathecal saline, HC, RRMS or SPMS CSF did not exhibit significant forelimb impairments, whereas those injected with PPMS CSF displayed motor deficits which persisted until 27 DPI (Supplementary Fig. 3A–D). At 12 days following lysolecithin injections, at a time when remyelination mechanisms are ongoing, PPMS CSF-injected mice had significantly larger demyelination volumes in the dorsal column and a longer rostral–caudal demyelination extent than other groups, suggesting that PPMS CSF impedes remyelination processes (one-way ANOVA, $P = 0.0230$ and $P = 0.0039$, respectively; Fig. 2A–C).

Lysolecithin-induced demyelination is accompanied by activation of astrocytes and microglia, which can have both detrimental and beneficial influences on remyelination by affecting OPC migration, proliferation and differentiation.[22-25] To determine whether PPMS CSF exacerbates glial activation, GFAP and Iba1 immunostaining was evaluated within the lesion in the dorsal column at 7 days post CSF injection. In PPMS CSF-injected mice, astrocytes were clearly more hypertrophic than in other groups and GFAP immunostaining intensity was significantly higher (one-way ANOVA, $P = 0.0001$; Fig. 2A and D). Similarly, microglial activation was exacerbated in PPMS CSF-injected mice, as shown by a greater abundance of amoeboid microglia and significantly higher Iba1 immunostaining intensity (one-way ANOVA, $P = 0.0059$; Fig. 2A and E). By 27 DPI, reactive astrogliosis and microglial activation had resolved, as GFAP and Iba1 expression were no longer upregulated in PPMS CSF-injected mice (Supplementary Fig. 3F and G).

To determine whether the delay in remyelination caused by PPMS CSF was due to reduced OPC proliferation and differentiation, the numbers of proliferating OPCs and mature oligodendrocytes were counted within the lesions. OPC proliferation, as

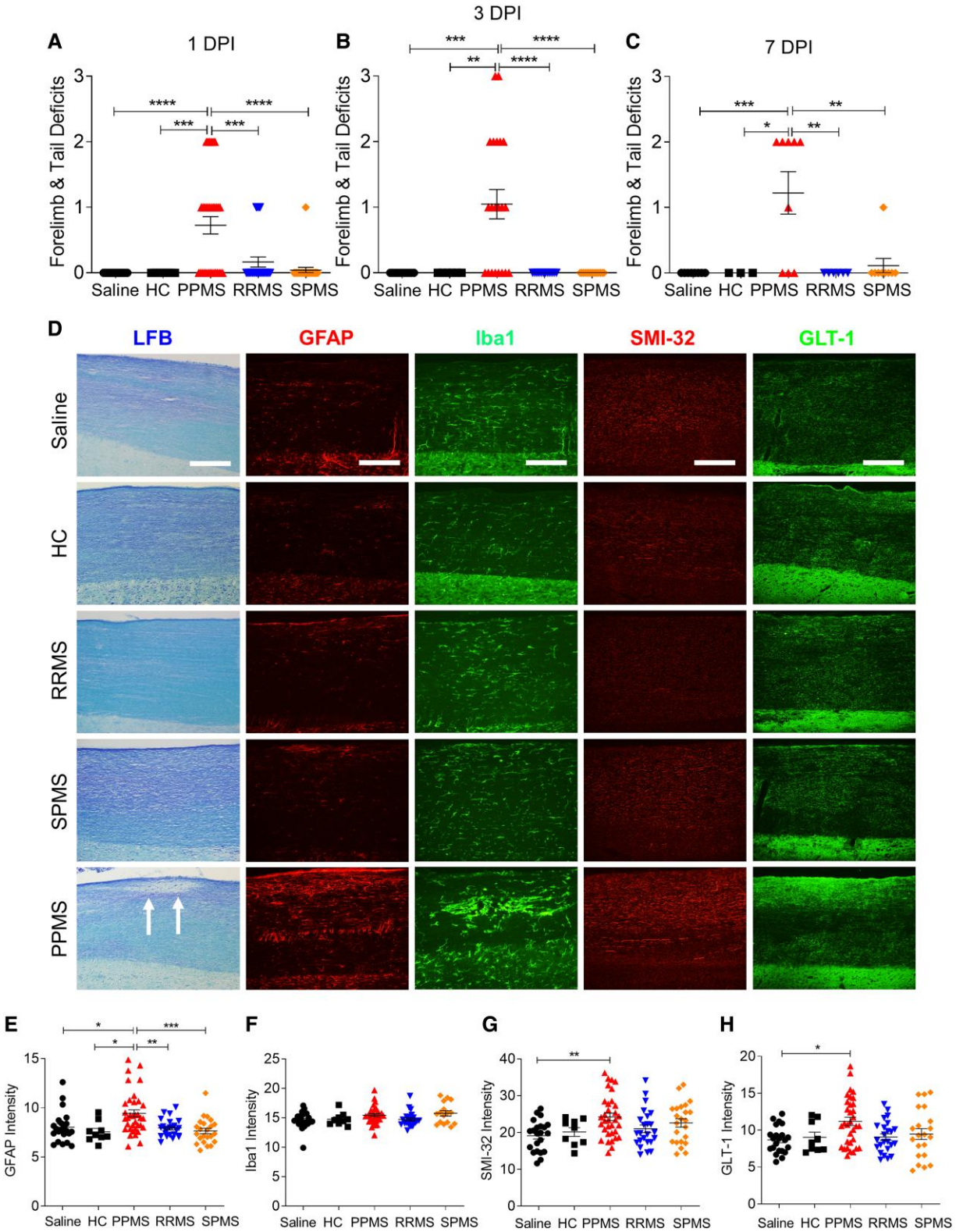

Figure 1 PPMS CSF induces motor deficits and spinal cord pathology. (**A**–**C**) Motor deficit scores at 1 (**A**), 3 (**B**) and 7 (**C**) days post intrathecal delivery of saline, CSF from healthy controls (HC; $n = 3$), or patients with PPMS ($n = 10$), RRMS ($n = 8$) or SPMS ($n = 8$). Each individual CSF sample listed in Table 1 was injected into a minimum of three mice. For 1 DPI: saline ($n = 20$ mice), HC ($n = 9$ mice), PPMS ($n = 33$ mice), RRMS ($n = 24$ mice), SPMS ($n = 24$ mice). For 3 DPI: saline ($n = 11$ mice), HC ($n = 6$ mice), PPMS ($n = 21$ mice), RRMS ($n = 12$ mice), SPMS ($n = 15$ mice). For 7 DPI: saline ($n = 8$ mice), HC ($n = 3$ mice), PPMS ($n = 9$ mice), RRMS ($n = 6$ mice), SPMS ($n = 9$ mice). PPMS CSF-injected mice exhibit significantly higher motor deficit scores than all other treatment groups. (**D**) Representative images of cervical spinal cords from different mice stained with LFB, GFAP, Iba1, SMI-32, or GLT-1 at 1 DPI. Arrows indicate demyelination in the dorsal white matter of PPMS CSF-injected mice. Scale bars = 100 µm. (**E**–**H**) Quantification of mean fluorescence intensities in the cervical spinal cord dorsal column white matter for GFAP immunostaining of astrocytes (**E**), Iba1 immunostaining of microglia (**F**), SMI-32 immunostaining of non-phosphorylated neurofilament H (**G**) and GLT-1 immunostaining of glutamate transporter-1 (**H**). Data plotted as mean ± SEM. Each point represents an individual mouse. One-way ANOVA with Bonferroni's test (**A**–**C** and **E**–**H**). $^{****}P < 0.0001$, $^{***}P < 0.001$, $^{**}P < 0.01$, $^{*}P < 0.05$.

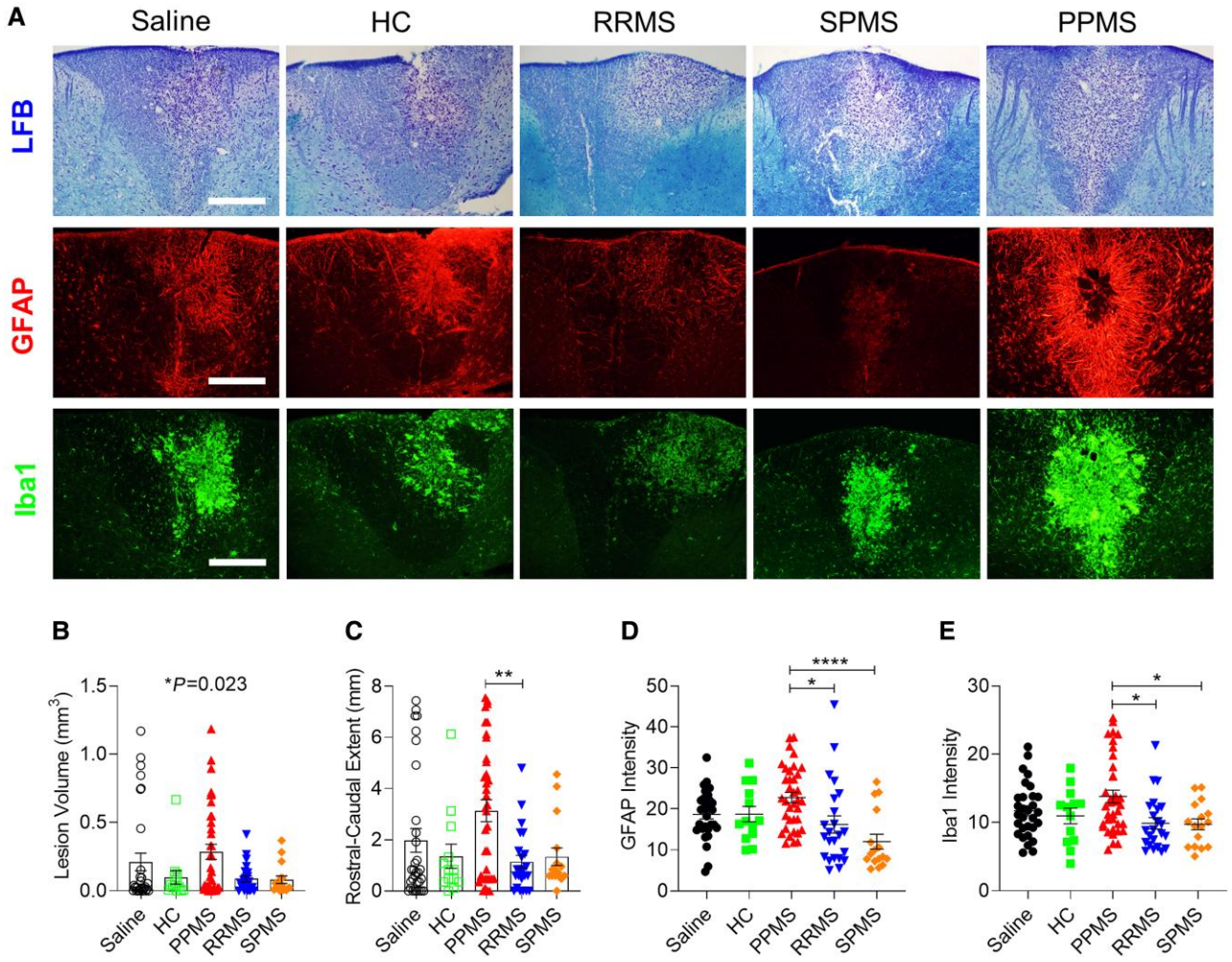

Figure 2 PPMS CSF delays remyelination and exacerbates reactive astrogliosis and microglial activation in lysolecithin-induced lesions. (**A**) Representative images of the dorsal column in cervical spinal cords stained with LFB, GFAP and Iba1 at 12 days post lysolecithin injection. Mice received intrathecal injections of saline or CSF from HC ($n = 3$), PPMS ($n = 8$), RRMS ($n = 7$) or SPMS patients ($n = 6$) listed in Supplementary Table 1 at 5 days post lysolecithin injection. Saline ($n = 31$ mice), HC ($n = 13$ mice), PPMS ($n = 36$ mice), RRMS ($n = 23$ mice), SPMS ($n = 16$ mice). Scale bars = 100 µm. (**B**) Total volume of demyelination in the cervical spinal cord determined by LFB staining. (**C**) Rostral–caudal extent of lesion determined by LFB staining. (**D**) Quantification of mean fluorescence intensity of GFAP$^+$ astrocytes throughout the lesion. (**E**) Quantification of mean fluorescence intensity of Iba1$^+$ microglia throughout the lesion. Data plotted as mean ± SEM. Each point represents an individual mouse. One-way ANOVA with Bonferroni's test (**B**–**E**). ****$P < 0.0001$, **$P < 0.01$, *$P < 0.05$.

determined by the number of NG2$^+$Ki67$^+$ cells, within the dorsal column lesion was similar among all groups (one-way ANOVA, $P = 0.2060$; Fig. 3A and B). Fewer APC$^+$Olig2$^+$ mature oligodendrocytes were found in the lysolecithin-induced lesions in PPMS CSF-injected mice (mean = 193) versus RRMS (mean = 229) and SPMS (mean = 236) (overall one-way ANOVA, $P = 0.0129$; Fig. 3C and D). This is consistent with a recent study reporting impaired OPC differentiation following *in vitro* exposure to progressive multiple sclerosis CSF.[26] By 27 DPI, remyelination within the lysolecithin lesion was evident in PPMS CSF-injected mice, indicating that although remyelination was delayed, it was not entirely blocked (Supplementary Fig. 3E).

CSF filtration attenuates motor deficits and spinal cord pathology in PPMS CSF-injected mice

To identify the pathogenic components in PPMS CSF responsible for inducing motor disability and spinal cord pathology, filtration studies were performed to eliminate PPMS CSF components by size, then unfiltered and filtered CSF samples were delivered intrathecally in mice. PPMS CSF samples underwent tangential flow filtration through 5 kDa or 100 kDa hollow fibre filters, which only allow components smaller than 5 kDa or 100 kDa to pass, respectively (Supplementary Table 2). Coomassie Blue staining confirmed accurate removal of CSF proteins by molecular weight following filtration (Fig. 4A). At 1 DPI, motor deficit scores were significantly lower (one-way ANOVA; $P = <0.0001$ for 5 kDa and 100 kDa) and normalized forelimb grip strength force was significantly stronger in mice injected with either 5 kDa or 100 kDa-filtered PPMS CSF compared to unfiltered PPMS CSF-injected mice (one-way ANOVA; $P = 0.0010$ for 5 kDa, $P = <0.0001$ for 100 kDa; Fig. 4B and D).

Next, we assessed whether the lack of motor deficit induction by filtered PPMS CSF was also accompanied by an attenuation in pathology. The capacity of PPMS CSF to induce demyelination, reactive astrogliosis and axonal damage was attenuated by filtration, as mice injected with either 5 kDa or 100 kDa-filtered PPMS CSF did

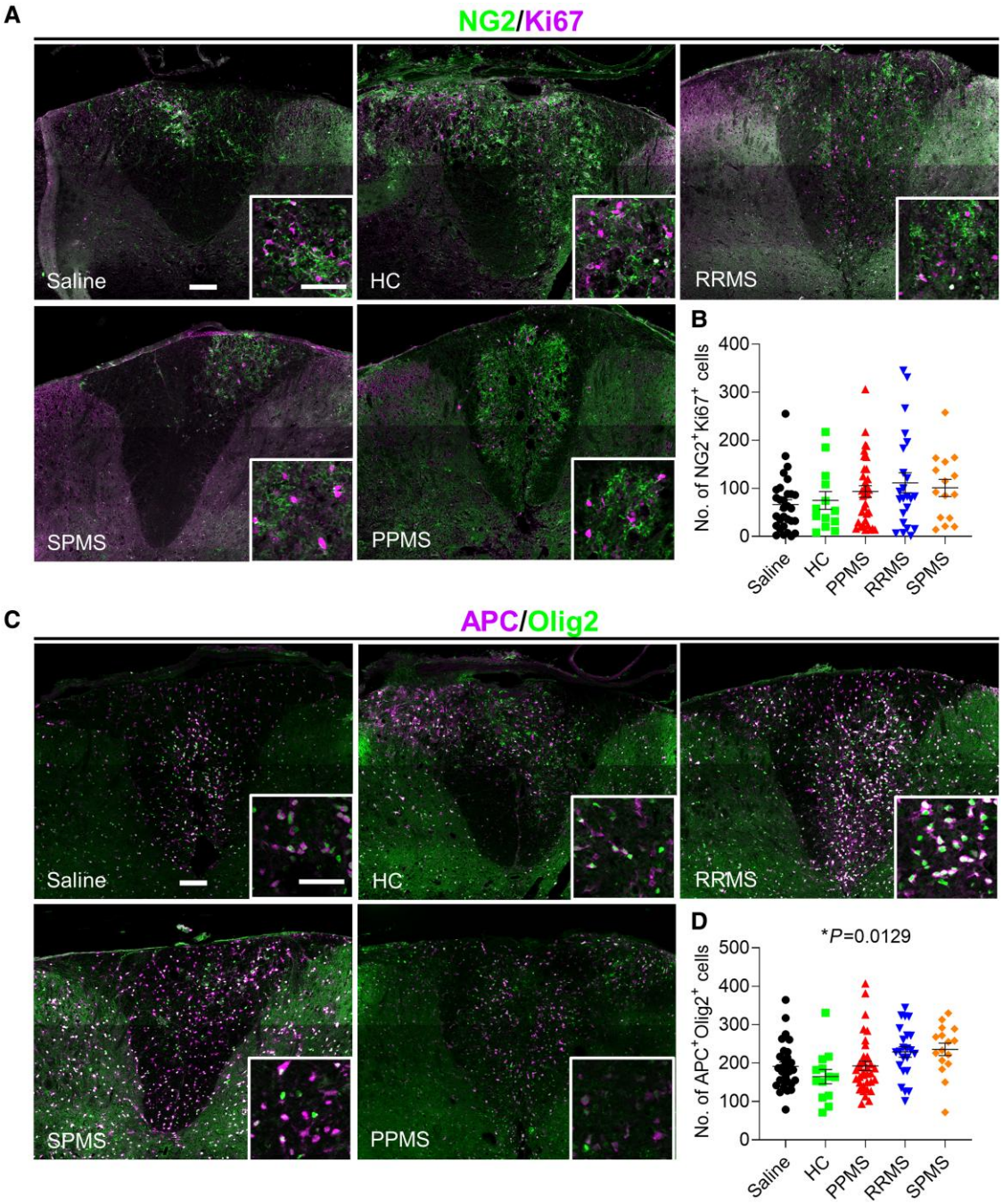

Figure 3 Fewer mature oligodendrocytes in lysolecithin-induced lesions in PPMS CSF-injected mice. (**A** and **C**) Representative images of the dorsal column in cervical spinal cords stained with NG2/Ki67 (**A**) and APC/Olig2 (**C**) at 12 days post lysolecithin injection. Mice received intrathecal injections of saline or CSF from HC ($n = 3$), PPMS ($n = 8$), RRMS ($n = 7$) or SPMS patients ($n = 6$) at 5 days post lysolecithin injection (Supplementary Table 1). Saline ($n = 31$ mice), HC ($n = 13$ mice), PPMS ($n = 36$ mice), RRMS ($n = 23$ mice), SPMS ($n = 16$ mice). Scale bars = 100 µm; inset = 50 µm. (**B**) Quantification of the number of $NG2^+Ki67^+$ proliferating OPCs throughout the lesion. (**D**) Quantification of the number of APC^+Olig2^+ mature oligodendrocytes throughout the lesion. Data plotted as mean ± SEM. Each point represents an individual mouse. One-way ANOVA with Bonferroni's test (**B** and **D**). $^*P < 0.05$.

not develop any demyelinated lesions in the cervical spinal cord, and both GFAP as well as SMI-32 expression were significantly lower compared to unfiltered PPMS CSF-injected mice (one-way ANOVA; GFAP $P = 0.0001$ for 5 kDa, $P = 0.0007$ for 100 kDa; SMI-32 $P = 0.0089$ for 5 kDa and $P = 0.0477$ for 100 kDa; Fig. 4E–I). Furthermore, filtered PPMS CSF was unable to enhance proliferation of primary human astrocytes as revealed by significantly fewer $GFAP^+Ki67^+$ proliferating human astrocytes in the 5 kDa-filtered PPMS CSF group compared to unfiltered PPMS CSF (t-test; $P = 0.0245$) and no increase in Ki67 mRNA levels (Supplementary Fig. 2G–I). The attenuation in PPMS CSF pathogenic capacity was not due to a general reduction in protein concentration, as CSF protein concentrations were similar following filtration through the 100 kDa filters (Fig. 4C). Taken together, these results suggest that filtration can effectively remove pathogenic components circulating in PPMS CSF and the size of the putative pathogenic component(s) is above 100 kDa.

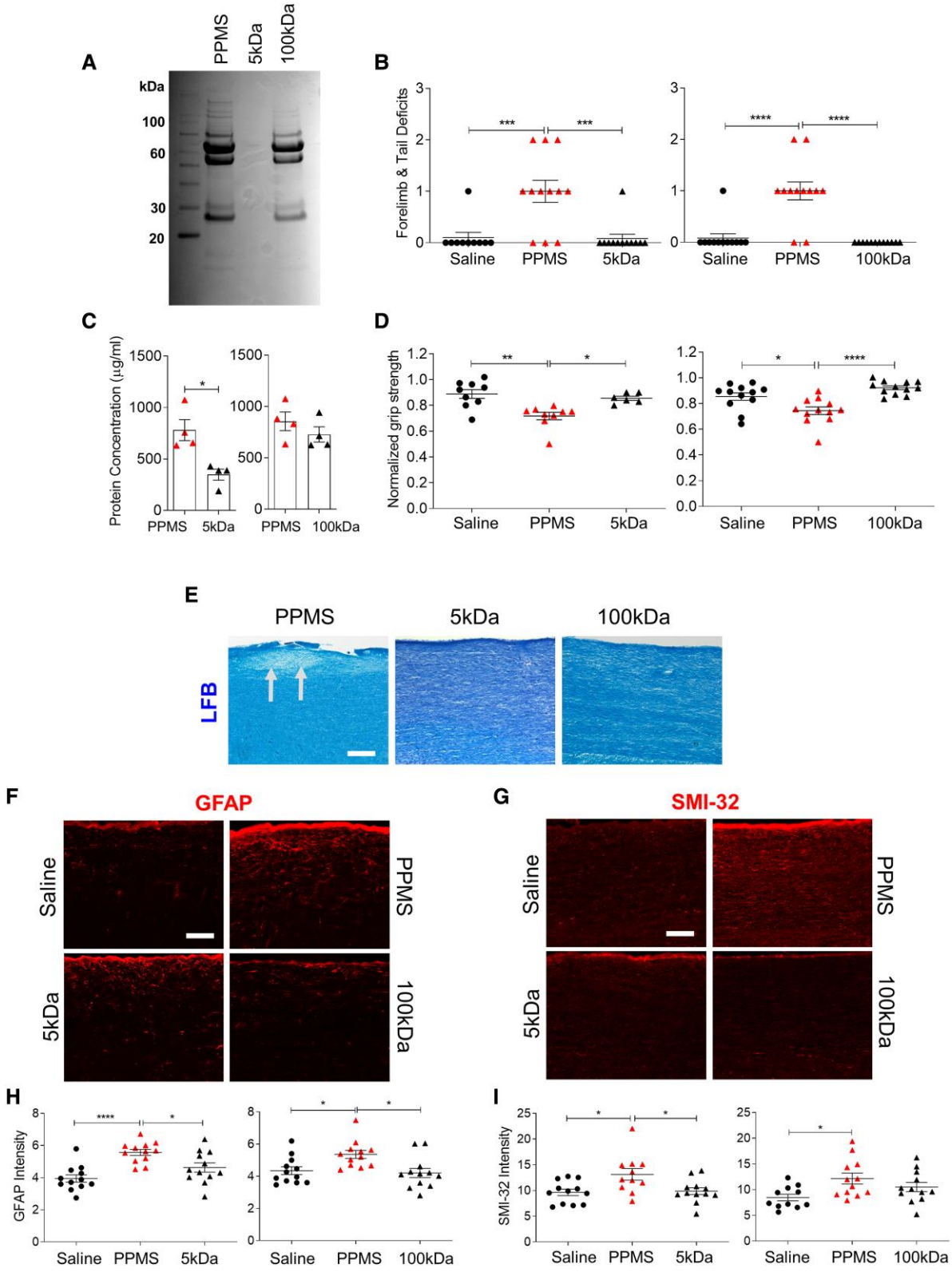

Figure 4 Filtration of PPMS CSF attenuates its pathogenic capacity. (**A**) Representative Coomassie Blue staining of an unfiltered PPMS CSF sample (PPMS), 5 kDa-filtered PPMS CSF (5 kDa) and 100 kDa-filtered PPMS CSF (100 kDa). Individual PPMS CSF samples were filtered through 5 kDa ($n = 4$) or 100 kDa ($n = 4$) MWCO hollow-fibre tangential flow filters (Supplementary Table 2). (**B**) Motor deficit scores at 1 DPI. Saline ($n = 15$ mice), PPMS CSF ($n = 18$ mice), 5 kDa-filtered PPMS CSF ($n = 12$ mice), 100 kDa-filtered PPMS CSF ($n = 12$ mice). (**C**) Total CSF protein concentration of unfiltered PPMS CSF and PPMS CSF passed through a 5 kDa hollow fibre tangential flow filter ($n = 4$) or 100 kDa filter ($n = 4$) for three filtration cycles. (**D**) Forelimb grip strength force at 1 DPI normalized to pre-surgery baseline force. (**E**) Representative images of LFB staining in the cervical spinal cord dorsal column at 1 DPI. Arrows indicate demyelination. (**F** and **G**) Representative images of GFAP immunostaining (**F**) and SMI-32 immunostaining (**G**) in the cervical spinal cord dorsal column at 1 DPI. (**H**) Quantification of mean fluorescence intensity of GFAP$^+$ astrocytes in the dorsal column. (**I**) Quantification of mean fluorescence intensity of SMI-32$^+$ axons in the dorsal column. Data plotted as mean ± SEM. Each point represents an individual CSF sample (**C**) or mouse (**B**, **D**, **H** and **I**). Paired Student's two-tailed *t*-test (**C**). One-way ANOVA with Bonferroni's test (**B**, **D**, **H** and **I**). $^{****}P < 0.0001$, $^{***}P < 0.001$, $^{**}P < 0.01$, $^{*}P < 0.05$. Scale bars = 100 µm.

IgG-depletion of PPMS CSF ameliorates motor deficits and spinal cord pathology

Because IgG oligoclonal bands (OCBs) in CSF are a diagnostic feature of multiple sclerosis[27] and IgGs have a molecular weight of 150 kDa, we investigated whether depletion of IgGs from PPMS CSF would mitigate its pathogenic capacity (Supplementary Table 2). Coomassie staining confirmed the reduction of immunoglobulin heavy and light chains in the IgG-depleted PPMS CSF (Fig. 5A). Mice injected with IgG-depleted PPMS CSF did not exhibit any motor deficits and forelimb grip strength force was unchanged from pre-surgery baseline at 1 DPI (one-way ANOVA, motor deficit scores: $P = 0.0012$; normalized grip strength: $P \leq 0.0001$; Fig. 5B and C). Histologically, IgG-depleted PPMS CSF-injected mice showed no evidence of demyelination, reactive astrogliosis or axonal damage in the cervical spinal cord. GFAP expression in mice injected with IgG-depleted PPMS CSF was similar to that of controls, indicating that IgG depletion can ameliorate effects of PPMS CSF on reactive astrogliosis (one-way ANOVA, $P = 0.0124$; Fig. 5D). SMI-32 expression was also similar between mice injected with IgG-depleted CSF and saline-injected mice (one-way ANOVA, $P = 0.6185$; Fig. 5E). These data strongly suggest that pathogenic IgGs in PPMS CSF are critically important for inducing motor disability and spinal cord pathology.

Intrathecal administration of PPMS recombinant antibodies induces motor deficits and spinal cord pathology

To further establish the role of pathogenic antibodies in PPMS disease pathophysiology, recombinant IgG_1 antibodies derived from B lymphocytes in CSF were produced and injected intrathecally into the cervical subarachnoid space in mice (Table 2 and Supplementary Tables 3 and 4). Mice injected with PPMS rAbs exhibited significantly higher motor deficit scores than mice injected with RRMS or SPMS rAbs, as well as mice injected with control rAbs derived from ALS and HTLV-1 patients (one-way ANOVA, $P \leq 0.0001$; Fig. 6A). Spiking 100 kDa-filtered PPMS CSF with an rAb from the same patient was able to recapitulate the detrimental effects of unfiltered PPMS CSF on motor function (Fig. 6F). Similar to the pathological changes induced by PPMS CSF, PPMS rAbs, but not RRMS or SPMS rAbs, induced reactive astrogliosis and axonal damage in the spinal cord (Fig. 6B, C and E). Antibodies from four of seven PPMS patients induced demyelination, whereas none of the rAbs from RRMS or SPMS patients caused demyelination (Fig. 6B). Additionally, PPMS rAb-injected mice exhibited upregulation of Iba1, suggesting that microglial activation is also induced by PPMS rAbs (Fig. 6D).

To determine whether human rAbs could be detected on mouse spinal cords following intrathecal delivery, human IgG immunostaining was performed on cervical spinal cords at 1 DPI. Human IgG staining was only observed with two out of four RRMS rAbs, while no positive immunostaining was detected in SPMS rAb or DC rAb-injected mice. However, a significantly higher incidence of human IgG staining was detected in PPMS rAb-injected mice as 10 out of 10 PPMS rAbs examined for human IgG staining showed positive IgG staining in the mouse spinal cord (Fig. 6B and Supplementary Fig. 4). Different human IgG staining patterns in PPMS rAb-injected mice were observed, including long axonal-like fibres in ventral white matter tracts, microglial-shaped cells in the grey matter and neuronal-shaped cells in the grey matter (Supplementary Fig. 4). Although we did not find evidence of specific antigen recognition, the increased presence of human IgG in PPMS rAb-injected spinal cords presumably facilitates the induction of motor disability and pathology. The increased human IgG staining in PPMS rAb-injected mice was not due to higher antibody concentration, as this was not significantly different between groups (Table 2).

Discussion

Multiple sclerosis is characterized as a primary demyelinating disorder whose cause is unknown. Genetic predisposition, infectious agents such as Epstein–Barr virus (EBV) as well as environmental factors are all implicated in the autoimmune disease pathogenesis. It is also undetermined whether the clinical phenotypes of RRMS (which may evolve to SPMS) and PPMS represent a single disease entity as the clinical manifestations of the two entities (RRMS/SPMS and PPMS) are quite distinct. Furthermore, the commonly used multiple sclerosis rodent model of EAE is associated with inflammatory demyelination similar to that seen in RRMS but does not accurately represent the clinicopathological features seen in PPMS. Previous attempts to transfer multiple sclerosis pathology to mice using RRMS CSF cells were unsuccessfully replicated,[28,29] and we previously demonstrated that progressive multiple sclerosis CSF can induce pathology in the brain.[17] This study describes the first CSF-induced animal model specific for PPMS. We used a novel approach involving intrathecal delivery of PPMS CSF into the cervical subarachnoid space, which resulted in rapid but persistent forelimb motor disability and hallmark multiple sclerosis pathology in the cervical spinal cord including: demyelination, impaired remyelination, reactive astrogliosis, microglial activation and axonal damage. Surprisingly, these pathological effects were not induced by CSF obtained from RRMS or SPMS patients, validating the specificity of our animal model for PPMS. In our recent study using a CSF-mediated animal model of sporadic amyotrophic lateral sclerosis (sALS), we reported that sALS CSF induces motor neuron degeneration whereas PPMS CSF does not, which further confirms the cellular disease specificity of our animal model.[30] Our finding that PPMS CSF-injected mice have fewer mature oligodendrocytes within a lysolecithin lesion is in agreement with a recent *in vitro* study reporting differential effects of CSF from RRMS and progressive multiple sclerosis patients, with impaired differentiation of cortical OPCs into mature oligodendrocytes only observed with progressive multiple sclerosis CSF (no distinction was made between SPMS and PPMS CSF).[26]

The clinicopathological observations in mice injected with CSF derived from PPMS patients were primarily driven by IgG antibodies, and not by cytokines, ceramides or other metabolites, as implicated in prior *in vivo* and *in vitro* studies.[15-17,31] We showed this by a series of experiments involving filtration and IgG depletion of CSF. Filtrate from the 5 kDa filters should have retained ceramides and metabolites, while the 100 kDa filtrate and IgG-depleted PPMS CSF should have retained ceramides and metabolites as well as cytokines, yet none of these samples were able to induce pathogenic effects in mice. Both filters should also have removed other immunoglobulins such as IgM and IgA as they are larger than 100 kDa, and although the Dynabeads™ Protein A have the highest affinity for IgG, they do have a low affinity for IgM and IgA; therefore, the possibility that other immunoglobulins in PPMS CSF may also be pathogenic cannot be excluded. Nevertheless, the entire clinical and pathological spectrum associated with intrathecal PPMS CSF injection into mice could be recapitulated by injecting recombinant IgG antibodies generated from PPMS patient CSF. Again, these findings did not occur with antibodies derived from RRMS/SPMS, suggesting that multiple sclerosis subtypes have distinct pathogenic processes. It was previously

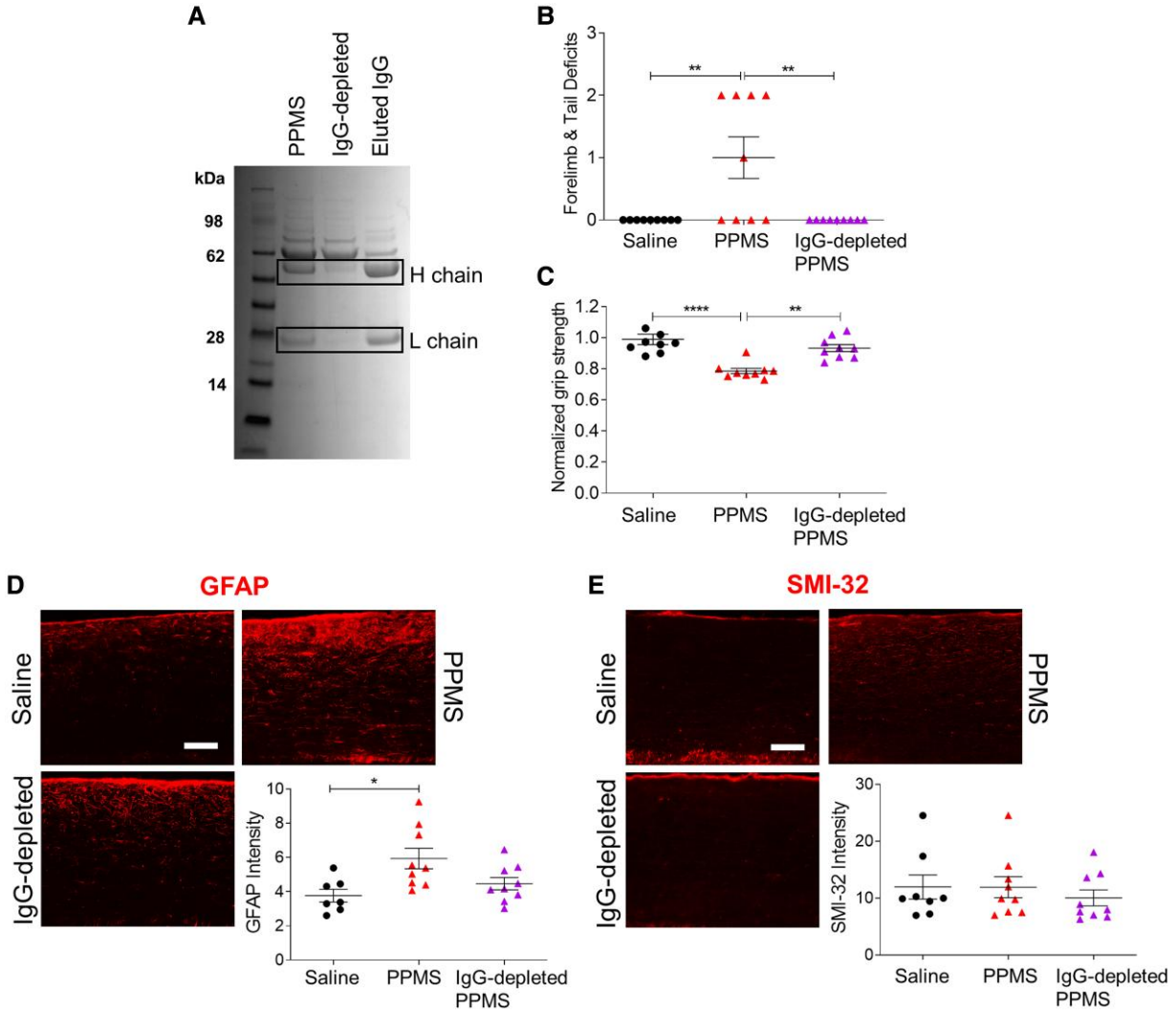

Figure 5 Depletion of IgG from PPMS CSF eliminates its pathogenic capacity. (**A**) Representative Coomassie Blue staining of a PPMS CSF sample, IgG-depleted PPMS CSF and the IgG eluted from the depletion. Individual PPMS CSF samples ($n = 3$) were incubated with Dynabeads™ Protein A to deplete IgGs (Supplementary Table 2). Boxes indicate presumptive positions of IgG heavy and light chains. (**B**) Motor deficit scores at 1 DPI. Saline ($n = 9$ mice), PPMS CSF ($n = 9$ mice), IgG-depleted PPMS CSF ($n = 9$ mice). (**C**) Forelimb grip strength force at 1 DPI normalized to pre-surgery baseline force. (**D**) Representative GFAP immunostaining images and quantification of mean fluorescence intensity in the cervical spinal cord dorsal column at 1 DPI. (**E**) Representative SMI-32 immunostaining images and quantification of mean fluorescence intensity in the cervical spinal cord dorsal column at 1 DPI. Data plotted as mean ± SEM. Each point represents an individual mouse. One-way ANOVA with Bonferroni's test (**B**–**E**). $^{****}P < 0.0001$, $^{**}P < 0.01$, $^{*}P < 0.05$. Scale bars = 100 µm.

reported that a subset of myelin-specific rAbs derived from RRMS patient CSF can cause demyelination in mouse organotypic cerebellar slices in a complement-dependent manner.[32] Although the pathogenic capacity of PPMS rAbs appears to be independent of (human) complement in our animal model, we cannot exclude the possibility that RRMS or SPMS rAbs may also be capable of inducing pathology in a complement-dependent manner.

A limitation of our PPMS CSF-induced animal model is the assumption that disease pathology arises from an upregulation of pathogenic factors in CSF as opposed to downregulation of protective factors necessary for maintaining healthy myelin and axons in the CNS. Although this study supports a role for intrathecal antibodies in PPMS CSF in mediating disease pathophysiology, we cannot exclude the possibility that depleted factors in PPMS CSF could also be contributing to disease pathology in PPMS.

A progressive model of multiple sclerosis previously developed in our laboratory required twice-weekly infusions of CSF into the third ventricle for several weeks before pathology was induced in the brain, and this injection paradigm failed to impair motor function.[17] In contrast, a single 3 µl PPMS CSF injection into the cervical subarachnoid space consistently induced functional deficits and pathology, suggesting that the spinal cord may be more vulnerable to PPMS CSF-induced damage than the brain. Interestingly, both PPMS and SPMS CSF caused pathological changes when infused into the brain, but only PPMS CSF induced spinal cord pathology when administered either via the third ventricle or the cervical subarachnoid space, perhaps suggesting regional specific disease mechanisms. Future studies should investigate whether PPMS and SPMS CSF-induced pathology in the brain are also antibody-mediated, or whether different pathogenic mechanisms are occurring in the brain *versus* the spinal cord.

Although CSF antibodies derived from RRMS or SPMS patients did not cause any discernible clinical or pathological effects in our model, despite being the same IgG_1 isotype as the PPMS rAbs and

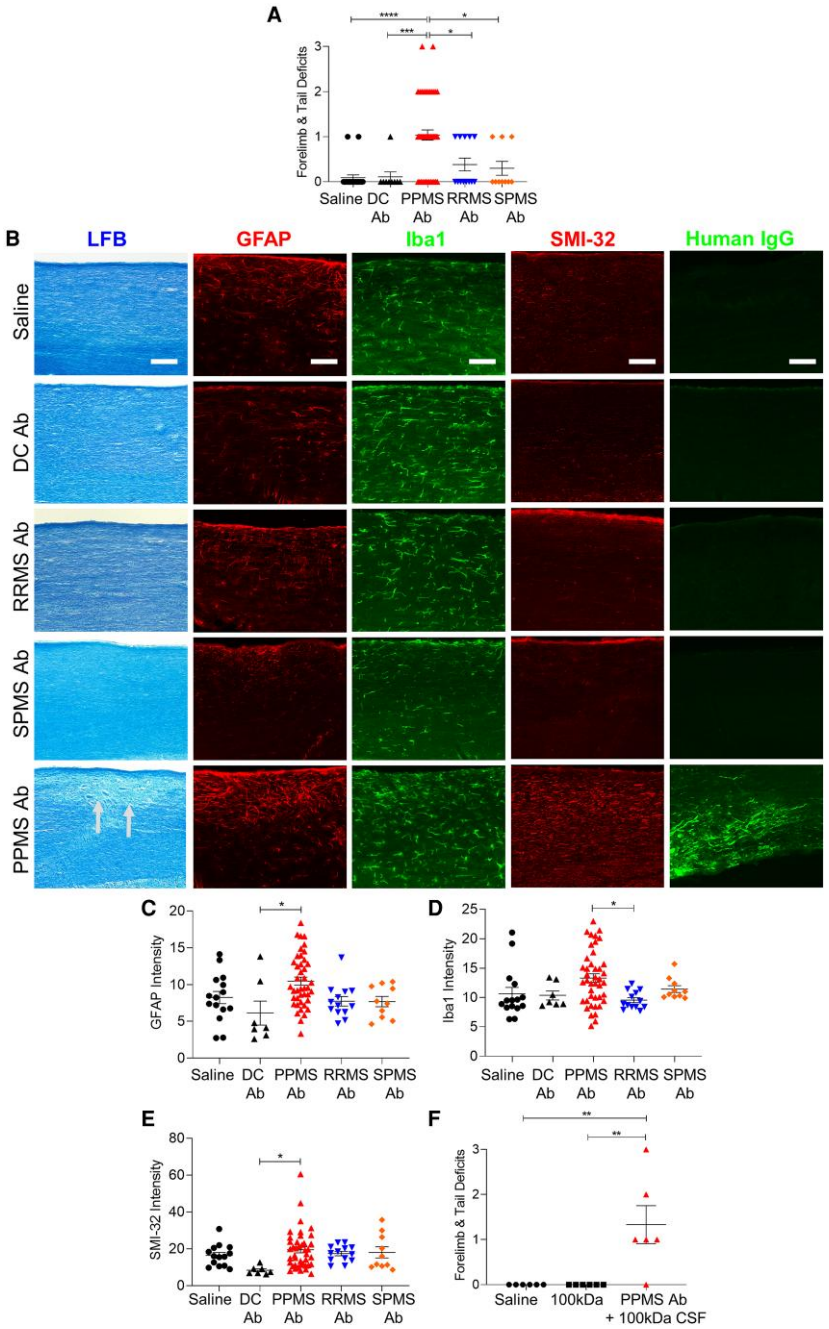

Figure 6 Pathogenic rAbs derived from B lymphocytes in PPMS CSF induce motor deficits and spinal cord pathology. (**A**) Motor deficit scores at 1 day post intrathecal delivery of rAbs derived from MS patients: PPMS ($n = 7$), RRMS ($n = 4$), SPMS ($n = 4$), and disease controls (DC): HTLV-1 ($n = 1$) and ALS ($n = 2$) (Table 2). Saline ($n = 22$ mice), DC rAbs ($n = 9$ mice), PPMS rAbs ($n = 51$ mice), RRMS rAbs ($n = 13$ mice), SPMS rAbs ($n = 10$ mice). (**B**) Representative images of cervical spinal cords stained with LFB, GFAP, Iba1, SMI-32, or human IgG at 1 DPI. Arrows indicate demyelination. Scale bars = 100 µm. (**C**) Quantification of mean fluorescence intensity of GFAP$^+$ astrocytes in the dorsal column. (**D**) Quantification of mean fluorescence intensity of Iba1$^+$ microglia in the dorsal column. (**E**) Quantification of mean fluorescence intensity of SMI-32$^+$ axons in the dorsal column. (**F**) Motor deficit scores of mice injected with saline ($n = 6$ mice), 100 kDa-filtered PPMS CSF ($n = 6$ mice) or PPMS rAbs added to 100 kDa-filtered PPMS CSF from the same patient ($n = 2$ PPMS patients, $n = 6$ mice) at 1 DPI. Data plotted as mean ± SEM. Each point represents an individual mouse. One-way ANOVA with Bonferroni's test (**A**, **C**–**F**). $^{****}P < 0.0001$, $^{***}P < 0.001$, $^{**}P < 0.01$, $^{*}P < 0.05$.

therefore capable of carrying out the same effector functions, our findings do not rule out their role in the disease. It is probable that autoantibodies are important in the pathogenesis of RRMS/SPMS because of the known response of such patients to B-cell-depleting therapies.[33] However, the pathogenic spectrum of RRMS/SPMS may involve T-cell–dependent mechanisms or other autoimmune pathways. Also, our cervical cord site of injections is better suited to investigate spinal cord disease rather than cerebral lesions as would be more pertinent with RRMS. Indeed, it may be argued that given our findings the response to anti-B-cell treatment in PPMS should be more convincing.[34] However, even in PPMS the OCBs in CSF persist despite B-cell-depleting treatments, suggesting that plasmablasts or plasma cells may be responsible for driving the intrathecal antibody response.[35] Identification of a single target

antigen of multiple sclerosis antibodies has been elusive and heterogeneous binding patterns of multiple sclerosis rAbs to different CNS antigens have been observed previously, suggesting they may be an epiphenomenon rather than the initial disease trigger.[36-38] Consistent with this, we also observed heterogeneous staining patterns in PPMS rAb-injected mice, but we found a higher incidence of human IgG staining in PPMS rAb-injected mice than RRMS and SPMS rAb-injected mice. This raises the possibility that pathogenic effects of PPMS rAbs perhaps arise from non-specific interaction with CNS tissue and the formation of immune complexes which may lead to the activation of IgG effector functions mediated by the fragment crystallizable (Fc) tail, rather than antigen-specific mechanisms involving the fragment antigen-binding (Fab) region.

The findings from this study are significant because our animal model relies on direct transmission of disease pathology using CSF from multiple sclerosis patients, which arguably mimics pathophysiological mechanisms occurring in patients with greater specificity than any currently existing animal model of multiple sclerosis. Direct comparison of pathogenicity of CSF from different multiple sclerosis subtypes revealed that PPMS may be an antibody-mediated autoimmune disease distinct from RRMS and SPMS. Because PPMS CSF antibodies create a toxic environment that causes demyelination, axonal damage and neurological dysfunction, repair strategies such as stem cell treatment are less likely to be efficacious in PPMS patients unless a specific treatment strategy aimed at intrathecal antibody depletion can be developed. Although further studies to better define the pathways by which autoantibodies cause the clinical spectrum in PPMS are needed, our study suggests that pathogenic antibodies play a unique role in PPMS. Furthermore, selective removal of antibodies from PPMS CSF via filtration or immunodepletion mitigates their pathogenic capacity in our experimental model, providing proof-of-concept to support CSF pheresis as a therapeutic approach for PPMS.

Acknowledgements

We thank Aaron McCabe, Laura Zitella Verbick and Natalie Nazarian at Minnetronix Neuro for providing equipment and guidance for the initial CSF filtration studies.

Funding

This study was supported by Tisch Multiple Sclerosis Research Center of New York (private funds).

Competing interests

The authors report no competing interests.

Supplementary material

Supplementary material is available at *Brain* online.

References

1. Lublin FD, Reingold SC. Defining the clinical course of multiple sclerosis: Results of an international survey. *Neurology*. 1996; 46:907-911.
2. Correale J, Gaitan MI, Ysrraelit MC, Fiol MP. Progressive multiple sclerosis: From pathogenic mechanisms to treatment. *Brain*. 2017;140:527-546.
3. Baecher-Allan C, Kaskow BJ, Weiner HL. Multiple sclerosis: Mechanisms and immunotherapy. *Neuron*. 2018;97: 742-768.
4. Thompson AJ, Kermode AG, Wicks D, *et al*. Major differences in the dynamics of primary and secondary progressive multiple sclerosis. *Ann Neurol*. 1991;29:53-62.
5. Revesz T, Kidd D, Thompson AJ, Barnard RO, McDonald WI. A comparison of the pathology of primary and secondary progressive multiple sclerosis. *Brain*. 1994;117:759-765.
6. Thompson AJ, Kermode AG, MacManus DG, *et al*. Patterns of disease activity in multiple sclerosis: Clinical and magnetic resonance imaging study. *BMJ*. 1990;300:631-634.
7. Kidd D, Thorpe JW, Thompson AJ, *et al*. Spinal cord MRI using multi-array coils and fast spin echo. *Neurology*. 1993;43: 2632-2637.
8. Rovaris M, Bozzali M, Santuccio G, *et al*. *In vivo* assessment of the brain and cervical cord pathology of patients with primary progressive multiple sclerosis. *Brain*. 2001;124:2540-2549.
9. Evangelou N, DeLuca GC, Owens T, Esiri MM. Pathological study of spinal cord atrophy in multiple sclerosis suggests limited role of local lesions. *Brain*. 2005;128:29-34.
10. Eden D, Gros C, Badji A, *et al*. Spatial distribution of multiple sclerosis lesions in the cervical spinal cord. *Brain*. 2019;142:633-646.
11. Lassman H, Bradl M. Multiple sclerosis: Experimental models and reality. *Acta Neuropathol*. 2017;133:233-244.
12. Constantinescu CS, Farooqi N, O'Brien K, Gran B. Experimental autoimmune encephalomyelitis (EAE) as a model for multiple sclerosis (MS). *Br J Pharmacol*. 2011;164:1079-1106.
13. Alcazar A, Regidor I, Masjuan J, Salinas M, Alvarez-Cermeno JC. Induction of apoptosis by cerebrospinal fluid from patients with primary progressive multiple sclerosis in cultured neurons. *Neurosci Lett*. 1998;255:75-78.
14. Haines J, Vidaurre OG, Zhang F, *et al*. Multiple sclerosis patient-derived CSF induces transcriptional changes in proliferating oligodendrocyte progenitors. *Mult Scler*. 2015;21: 1655-1669.
15. Vidaurre OG, Haines JD, Sand IK, *et al*. Cerebrospinal fluid ceramides from patients with multiple sclerosis impair neuronal bioenergetics. *Brain*. 2014;137:2271-2286.
16. Wentling M, Lopez-Gomez C, Park H, *et al*. A metabolic perspective on CSF-mediated neurodegeneration in multiple sclerosis. *Brain*. 2019;142:2756-2774.
17. Cristofanilli M, Rosenthal H, Cymring B, *et al*. Progressive multiple sclerosis cerebrospinal fluid induces inflammatory demyelination, axonal loss, and astrogliosis in mice. *Exp Neurol*. 2014;261:620-632.
18. Thomspon AJ, Banwell BL, Barkhof F, *et al*. Diagnosis of multiple sclerosis: 2017 revisions of the McDonald criteria. *Lancet Neurol*. 2018;17:162-173.
19. Stevenson VL, Leary SM, Losseff NA, *et al*. Spinal cord atrophy and disability in MS. *Neurol*. 1998;51:234-238.
20. Bjartmar C, Kidd G, Mörk S, Rudick R, Trapp BD. Neurological disability correlates with spinal cord axonal loss and reduced N-acetyl aspartate in chronic multiple sclerosis patients. *Ann Neurol*. 2000;48:893-901.
21. Werner P, Pitt D, Raine CS. Multiple sclerosis: Altered glutamate homeostasis in lesions correlates with oligodendrocyte and axonal damage. *Ann Neurol*. 2001;50:169-180.
22. Bannerman P, Hahn A, Soulika A, Gallo V, Pleasure D. Astrogliosis in EAE spinal cord: Derivation from radial glia, and relationships to oligodendroglia. *Glia*. 2007;55:57-64.
23. Williams A, Piaton G, Lubetzki C. Astrocytes—Friends or foes in multiple sclerosis? *Glia*. 2007;55:1300-1312.
24. Correale J, Farez MF. The role of astrocytes in multiple sclerosis progression. *Front Neurol*. 2015;6:180.

25. Miron VE, Boyd A, Zhao J, *et al*. M2 microglia and macrophages drive oligodendrocyte differentiation during CNS remyelination. *Nat Neurosci*. 2013;16:1211-1218.
26. Zviek O, Fainstein N, Rechtman A, *et al*. Cerebrospinal fluid of progressive multiple sclerosis patients reduces differentiation and immune functions of oligodendrocyte progenitor cells. *Glia*. 2022;70:1191-1209.
27. Stangel M, Fredrikson S, Meinl E, Petzold A, Stüve O, Tumani H. The utility of cerebrospinal fluid analysis in patients with multiple sclerosis. *Nat Rev Neurol*. 2013;9:267-276.
28. Saeki Y, Mima T, Sakoda S, *et al*. Transfer of multiple sclerosis into severe combined immunodeficiency mice by mononuclear cells from cerebrospinal fluid of the patients. *Proc Natl Acad Sci U S A*. 1992;89:6157-6161.
29. Hao Q, Saida T, Nishimura M, Ozawa K, Saida K. Failure to transfer multiple sclerosis into severe combined immunodeficiency mice by mononuclear cells from CSF of patients. *Neurology*. 1994;44:163-165.
30. Wong JK, Roselle AK, Shue TS, *et al*. Apolipoprotein B-100-mediated motor neuron degeneration in sporadic amyotrophic lateral sclerosis. *Brain Commun*. 2022;4:fcac207.
31. Nntranos A, Park H, Wentling M, *et al*. Bacterial neurotoxic metabolites in multiple sclerosis cerebrospinal fluid and plasma. *Brain*. 2022;145:569-583.
32. Liu Y, Given KS, Harlow DE, *et al*. Myelin-specific multiple sclerosis antibodies cause complement-dependent oligodendrocyte loss and demyelination. *Acta Neuropathol Comm*. 2017;5:25.
33. Hauser SL, Bar-Or A, Comi G, *et al*. Ocrelizumab versus interferon beta-1a in relapsing multiple sclerosis. *N Engl J Med*. 2017;376:221-234.
34. Montalban X, Hauser SL, Kappos L, *et al*. Ocrelizumab versus placebo in primary progressive multiple sclerosis. *N Engl J Med*. 2017;376:209-220.
35. Greenfield AL, Dandekar R, Ramesh A, *et al*. Longitudinally persistent cerebrospinal fluid B cells can resist treatment in multiple sclerosis. *JCI Insight*. 2019;4:e126599.
36. Hohlfeld R, Dornmair K, Meinl E, Wekerle H. The search for the target antigens of multiple sclerosis, part 2: CD8+ T cells, B cells, and antibodies in the focus of reverse-translational research. *Lancet Neurol*. 2016;15:317-331.
37. Owens GP, Bennett JL, Lassmann H, *et al*. Antibodies produced by clonally expanded plasma cells in multiple sclerosis cerebrospinal fluid. *Ann Neurol*. 2009;65:639-649.
38. Blauth K, Soltys J, Matschulat A, *et al*. Antibodies produced by clonally expanded plasma cells in multiple sclerosis cerebrospinal fluid cause demyelination of spinal cord explants. *Acta Neuropathol*. 2015;130:765-781.